An Integrated Process–Failure Simulation Framework for Predicting Composite Allowables via Multi-Fidelity Stochastic Simulation and Machine Learning

Amirali Eskandariyun[1], Huilong Fu[1], Navid Zobeiry[1*]

[1] University of Washington, Seattle WA 98195, USA
*Corresponding Author: navidz@uw.edu

Peer-reviewed Version of Record: Eskandariyun, A., Fu, H., and Zobeiry, N. (2026). An integrated process–failure simulation framework for predicting composite allowables via multi-fidelity stochastic simulation and machine learning. Composites Part B: Engineering, 326, 114051. https://doi.org/10.1016/j.compositesb.2026.114051

Abstract. For material screening, qualification, and certification of aerospace composites, it is essential to establish statistical design properties that account for both inherent material variability and process-induced uncertainty. Regulatory standards require the determination of A-basis and B-basis statistical values as conservative lower bound design allowables. At present, allowables are determined through extensive experimental campaigns, which are costly and time-consuming, thereby limiting the exploration of new material systems. In this work, we present a multiscale, multi-fidelity process-failure modeling framework that enables the digital prediction of allowables. The framework integrates thermo-chemical-mechanical process simulations with stochastic multi-fidelity failure simulations to capture the effects of curing-induced properties, residual stresses, and microstructural variability on mechanical performance. Machine learning surrogate models, trained via transfer learning, accelerate uncertainty propagation across scales, while Bayesian inference leverages limited experimental data to quantify uncertain parameters. High-fidelity macroscale failure simulations then predict tensile strength distributions from which A- and B-basis allowables are estimated. Application to Hexcel AS4/8552 cross-ply laminates demonstrates close agreement with test data, with conservative predictions of statistical allowables. By combining stochastic process-failure simulations with machine learning, this framework establishes a predictive pathway for estimating allowables and reducing the extent of costly experiments required during composite qualification and certification.

Keywords: Process Simulation, Failure Simulation, Bayesian Inference, Machine Learning, Allowables, Aerospace Certification

1 Introduction

Composite materials, particularly carbon fiber–reinforced polymers (CFRPs), have become indispensable in modern aerospace structures due to their exceptional specific stiffness and strength, corrosion resistance, and design flexibility [1–3]. Aircraft such as the Boeing 787 and Airbus A350 utilize more than 50% composites by weight, enabling improvements in fuel efficiency and performance, as well as accelerating the assembly rate due to part consolidation [4]. However, the widespread adoption of composites in safety-critical structures is constrained by challenges in predicting their performance under various conditions. Unlike metals, which exhibit relatively homogeneous and predictable properties, composite performance depends on material variability and complex interactions between fibers, matrix, and layers across multiple length scales, as well as uncertainties during processing [5–7].

To ensure safety and reliability, aerospace certification requires establishing statistical design properties that capture both material variability and processing uncertainty through repeated coupon-level experiments. These values, known as design allowables, are conservative lower bounds used in structural design. Specifically, the A-basis allowable corresponds to the 1st percentile of the property distribution with 95% confidence, while the B-basis allowable corresponds to the 10th percentile with 95% confidence [8,9]. These allowables are fundamental to the design and certification of composite structures, yet they are currently obtained exclusively through comprehensive testing campaigns [10].

The experimental "building block" approach, in which thousands of coupons, elements, and subcomponents are tested across different batches, layups, and environmental conditions, is both time-consuming and expensive [11,12]. Such efforts are typically integrated across multiple stages of design and can span several years. While this costly approach is essential for certifying the airworthiness of composite aircraft, it significantly constrains the exploration of novel materials and manufacturing processes [13]. Although the certification approach based on analysis supported by testing requires extensive simulations at every level of the building block pyramid [9], design allowables are still determined from extensive testing to account for material and process variabilities. A predictive, simulation-informed pathway to estimate statistical design values, including A- and B-basis allowables, would therefore represent a transformative step in the certification of aerospace composites [13–15].

A major barrier is the multiscale and stochastic origin of uncertainty in composites. Variability arises at the constituent level, where fiber and matrix respective properties and microstructural morphology may vary [16–18]. These local variations, coupled with processing variability, propagate across plies and laminates, manifesting as scatter in macro responses [19,20]. In practice, integrated process and failure analyses are rarely conducted, and even when they are, it remains difficult to represent the complex nature of material and process variability or the effects of manufacturing defects [21–27]. Capturing such effects requires stochastic analyses informed by the underlying distributions and correlations of these uncertainties which are often unavailable. Process-induced effects such as residual stresses and porosity further contribute to variability [28–30]. As a result, single-scale or homogenized models cannot adequately represent these cascades of uncertainty. Hence, an integrated process-failure simulation framework must operate stochastically across scales to track how small-scale variability influences material performance [31–33].

Equally challenging is the trade-off between predictive fidelity and computational cost. High-fidelity micromechanical Finite Element (FE) simulations can capture the underlying physical mechanisms, but their computational cost prohibits their use in large stochastic analyses [34,35]. Conversely, low-fidelity or reduced-order models are computationally efficient but lack sufficient accuracy for certification-relevant predictions [36]. Multi-fidelity modeling, which combines the efficiency of low-fidelity simulations with the accuracy of high-fidelity ones, has emerged as a promising strategy [37,38]. Machine learning–based surrogate models can further integrate these fidelity levels, enabling efficient quantification and propagation of uncertainties across scales and throughout processing and failure stages, while retaining physics-based accuracy [39–42].

A related challenge lies in representing manufacturing uncertainties through process simulations. Composite properties are strongly affected by thermo-chemo-mechanical events during processing. For example, in thermoset composites processed in autoclaves, variations in heat transfer, resin flow, fiber-bed compaction, and degree of cure evolution, together with the development of residual stresses, directly influence the microstructure and behavior of the cured material, ultimately contributing to scatter in mechanical response [43–45]. Processing defects are another source of uncertainty in composites. Numerous studies have demonstrated that porosity, fiber waviness, and other manufacturing-induced anomalies significantly degrade mechanical properties such as stiffness, strength, and fatigue life [13,46]. Hence, explicitly incorporating process physics into uncertainty quantification is essential to link manufacturing variability with failure behavior [47,48].

Recent advances in machine learning (ML) have further expanded opportunities for predictive modeling of both process and failure in composites [49,50]. However, purely data-driven approaches, may face challenges due to limited experimental datasets, fragmented data sources, and a lack of physical interpretability. In contrast, physics-based simulations provide mechanistic fidelity but are computationally expensive. A hybrid approach, in which machine learning accelerates physics-based simulations, offers a compelling balance between efficiency and physical consistency, enabling interpretable uncertainty quantification [51–53].

In this work, we address these challenges by developing a unified stochastic process–failure simulation framework for estimating statistical allowables in aerospace composites. The framework combines multiscale simulations, multi-fidelity modeling, and machine learning to quantify uncertainties and their effects on statistical performance of composites. Additionally, our approach leverages limited experimental data for calibration and uncertainty quantification. This enables digital prediction of A- and B-basis allowables, offering a new pathway to reduce experimental demands and accelerate certification.

2 Methodology

2.1 Workflow Overview

As illustrated in **Fig. 1**, the workflow combines process simulations, stochastic multiscale failure analyses, ML surrogate modeling, and Bayesian inference to efficiently quantify and propagate uncertainties across scales and digitally estimate A- and B-basis allowables. The workflow consists of eight sequential steps, which are explained in detail below, and are explicitly identified in **Fig. 1**:

(1) Prior Distributions

The workflow begins by defining probabilistic input distributions for key material and process parameters, including resin weight fraction, fiber aerial weight, and heat transfer coefficients. Since most of these distributions cannot be characterized exactly, we first define realistic ranges informed by available data. These prior distributions are subsequently refined through calibration using observations from our experimental tests.

(2) Cured Ply-Thickness Distribution Estimation

Using the prepreg prior distributions of properties (fiber areal weight, FAW, and matrix weight fraction, W_m), we estimate the cured ply thickness and verify against experimental data if available.

(3) Stochastic Macroscale Thermo-Chemical Process Simulation

In this step, we perform stochastic 1D macroscale thermo-chemical process simulations through the thickness of both the part and the tool, accounting for convective heating in an autoclave. The temperature cure cycle, the cured ply-thickness, the lay-up, the tooling material, and the tooling thickness are all modeled explicitly. Heat-transfer-coefficient distributions above the part and beneath the tool are also incorporated. Each simulation samples from probabilistic inputs to capture natural variability in the thermal and cure response. Using these inputs, we compute the through-thickness temperature history and the degree-of-cure evolution. This analysis requires a cure-kinetics model for the resin and total heat-of-reaction, along with temperature- and cure-dependent thermal properties of the resin, fiber, and tool (conductivity and specific heat). In this study, these parameters are treated as fixed values (i.e., not assigned probabilistic distributions). The resulting temperature and cure histories enable prediction of the evolving composite mechanical properties in subsequent steps.

(4) Microscale RVE Generation

To continue the multiscale workflow, we generate 2D realistic local microstructures to serve as the microscale Representative Volume Element (RVE). We use a Smoothed Particle Hydrodynamics (SPH)-based packing algorithm to simulate the random distribution of fibers within the RVE, following the methodology developed by Husseini et al. [54]. This produces statistically representative microstructures that reflect realistic fiber spacing and packing variability.

(5) Stochastic Microscale Thermo-Mechanical Process Simulation

Given the generated RVEs and the temperature and degree-of-cure histories from the 1D thermo-chemical simulation, we perform a 2D microscale thermo-mechanical analysis. Cure Hardening Instantaneously Linear Elastic (CHILE) method [55,56], which is a pseudo-viscoelastic constitutive model, is employed to track the evolution of residual stresses and cured material properties within the heterogeneous microstructure. For stochastic analysis, variations in evolution of properties during cure, including modulus, cure shrinkage, and coefficient of thermal expansions are considered.

(6) Stochastic Microscale Failure Simulation (High and Low-Fidelity)

Using the predicted residual-stresses, we perform stochastic microscale failure simulations at two fidelity levels. High-fidelity models resolve detailed fracture mechanics and local failure modes, while low-fidelity models provide computationally efficient approximations suitable for large-scale sampling. Data generation continues until a sufficiently large database is built to characterize the statistical distribution of microscale strength and failure behavior.

 VOR: doi.org/10.1016/j.compositesb.2026.114051

(7) Multi-Fidelity Surrogate Modeling and Bayesian Uncertainty Calibration

Once the simulation database is established, a multi-fidelity surrogate model is trained and used to perform uncertainty quantification through Bayesian inference-based calibration. The model predictions are combined with experimental transverse-tension data, and a Markov Chain Monte Carlo (MCMC) procedure is used to update the uncertain input parameters. This calibration step ensures that the simulated responses are statistically consistent with the experimental observations and produces posterior input distributions that reflect true material and process variability.

(8) Uncertainty Propagation and Allowables Prediction

Finally, the calibrated (posterior) input distributions are propagated through the entire stochastic process–failure simulation framework. By repeatedly sampling these inputs, running the multiscale workflow, and performing a high-fidelity macroscale failure simulation of a cross-ply laminate, we generate probabilistic strength distributions and compute the corresponding A- and B-basis allowables. The predicted allowables are then compared against cross-ply experimental results to validate the full framework.

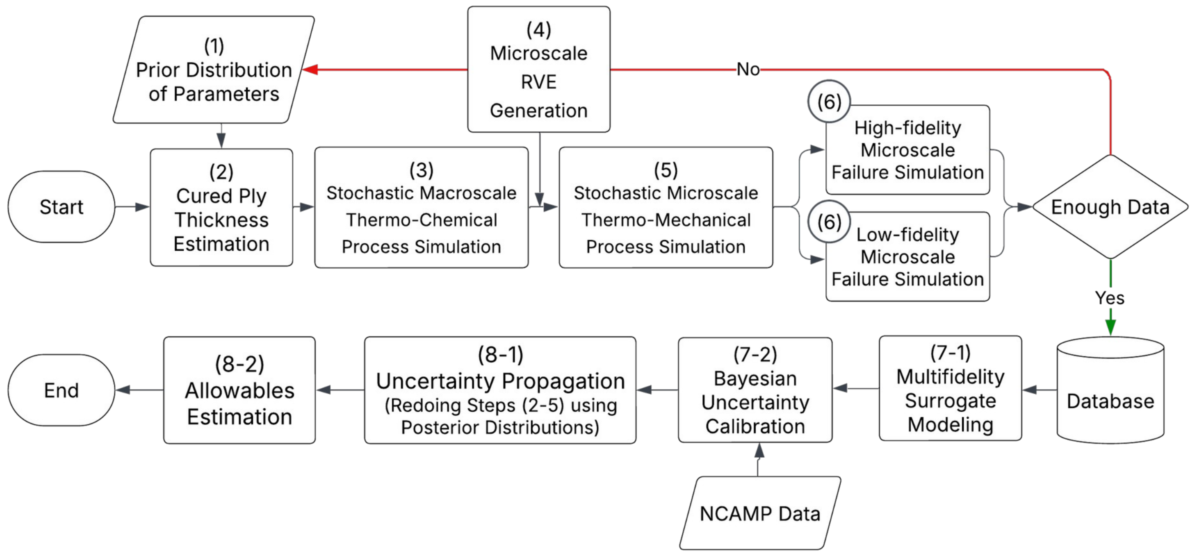

Fig. 1. The flowchart representing the presented eight-step workflow used to predict statistical allowables in composites through integrated multiscale process-failure simulations and machine learning.

2.2 Thermo-Chemical & Thermo-Mechanical Process Modeling

Upon defining the probabilistic input ranges and determining the ply thicknesses, the decoupled multiscale process simulation proceeds in two stages: (i) stochastic 1D thermo-chemical simulation of the tool–part system at the macroscale, followed by (ii) stochastic microscale thermo-mechanical analysis of the prepreg to evaluate residual stress.

This study employs a one-dimensional process simulation framework to model the curing of composite laminates in an autoclave, considering coupled conduction and convective heat transfer, and polymerization heat generation during cure. At each FE time step, the model solves for temperature and degree of cure, from which the glass-transition temperature (T_g) and all temperature-/cure-dependent properties are updated, including cure shrinkage, thermal expansion coefficients, specific heat capacity, thermal conductivity, and the evolving resin/lamina modulus. This simulation therefore predicts the through-thickness evolution of key properties such as degree of cure, T_g, modulus, and cure shrinkage over the thermal cycle [57].

Finally, residual stresses generated during cure are estimated using the CHILE pseudo-viscoelastic model at the microscale, which accounts for cure-dependent modulus evolution and mismatch of free strains [34]. Other contributing factors including tool-part interaction during cure are ignored in this analysis. In **Fig. 2** below, a schematic representation of the macroscale 1D autoclave cure simulation and a sample for the 2D microstructure and residual stress buildup are shown.

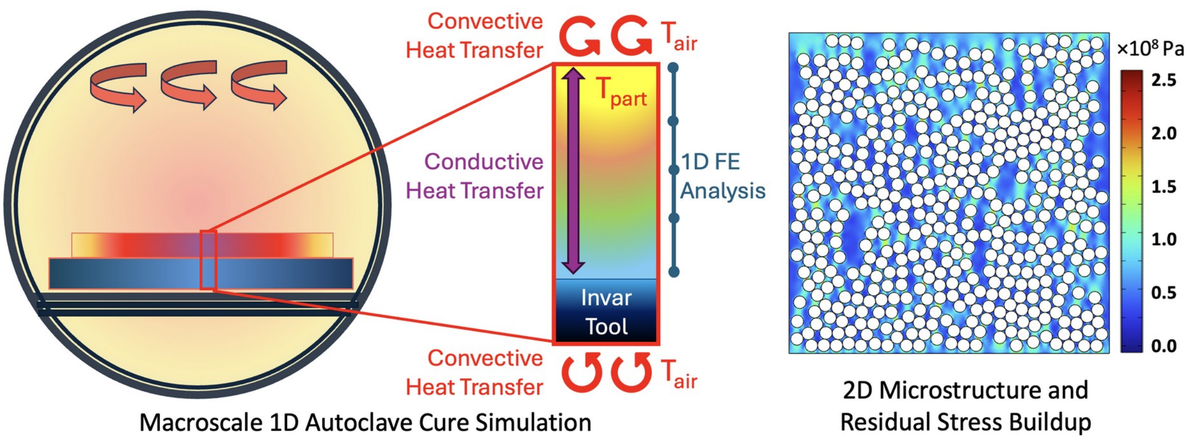

Fig. 1. Schematic of thermo-chemical-mechanical process simulation and sample results for distribution of residual stresses at the micro scale.

To analyze the curing behavior of composite, stochastic one-dimensional thermo-chemical simulations were conducted through the thickness of the part and tool, while subjected to convective heating (See **Fig. 2**). In addition to cure kinetics model and resin heat of reaction, thermal properties of tool and part, as well as physical prepreg properties such as matrix weight fraction and thickness are needed. In this study, for stochastic analysis, only heat transfer coefficients and prepreg physical properties were varied, while thermal properties were considered constant. However, variation in other parameters can also be included using the same framework.

Next, to capture the development of residual stresses during the curing, CHILE method was implemented for thermo-mechanical analysis where residual stress $\sigma(t)$ is computed by:

$$\sigma(t) = \int_0^t E'(T,\ \alpha)\ \frac{d\varepsilon - d\varepsilon_{free}}{d\tau} d\tau \tag{1}$$

In this formulation, $E'(T,\ \alpha)$ is the storage modulus of the resin as a function of temperature (T) and degree of cure (α). The term ε refers to the total strain, while ε_{free} denotes the strain induced by thermal expansion/shrinkage and cure shrinkage.

Fig. 3 illustrates the schematic representation of the cure process and displays representative results, including the air (T_{air}) and part (T_{part}) temperature histories, along with the evolution of the degree of cure (DoC) and T_g throughout the cure cycle. The simulation outputs the evolution of residual stresses during the curing process. In this figure, the volume-averaged residual stress at each instant is shown for the entire microstructural RVE.

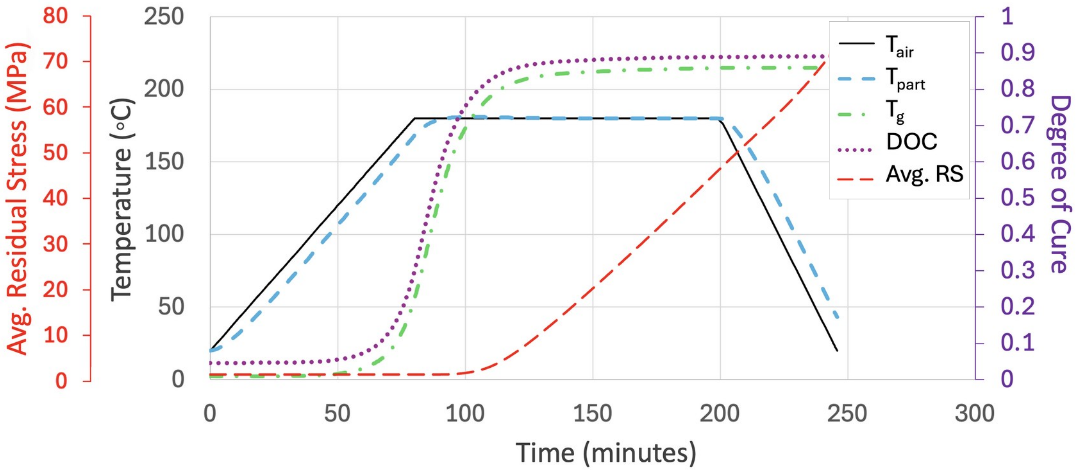

Fig. 1. Thermo-chemical cure history (air and part temperatures, DoC, and T_g) together with the corresponding thermo-mechanical response, shown here as the evolution of the volume-averaged residual stress predicted using the CHILE model.

2.3 Multi-fidelity Microscale Failure Simulation

For this phase of the simulation process, we employed a Continuum Damage Mechanics (CDM) approach in combination with the Crack Band Fracture Model (CBFM) at two distinct fidelity levels defined by the discretization density. The CBFM is a strain-softening, fracture-energy–regularized constitutive framework, originally introduced by Bažant and Oh (1983) [29], that ensures numerical objectivity by relating the softening response to a characteristic material length scale. This framework is particularly suited for capturing localized failure mechanisms within the constituent phases, as it ensures that damage localization within an element dissipates the correct amount of fracture energy.

For computational implementation, we employed the COMSOL Multiphysics FE package. The realistic RVEs, generated using SPH analysis, were reconstructed in COMSOL at two resolutions. A coarser mesh consisting of approximately 25000 triangular elements was used for the lower-fidelity simulations, while a finer mesh of approximately triangular 400000 (~16 times the low-fidelity) elements was used for the high-fidelity simulations. A linear softening law was adopted for the matrix constituents, where the ultimate failure strain was calibrated based on matrix fracture energy and element characteristic length, following the CBFM regularization procedure [29,58,59]. For the failure simulation, we constrained the RVE nodes on one side in the horizontal direction and applied a tensile displacement corresponding to 2% strain on the opposite side along the same axis.

Each failure simulation required approximately 2–3 minutes for the low-fidelity case and 10–15 minutes for the high-fidelity case on a standard computer workstation with an Intel Core i9-12900K processor and 64 GB of RAM. A representative RVE configuration and corresponding meshes are shown in **Fig. 4** For comparison.

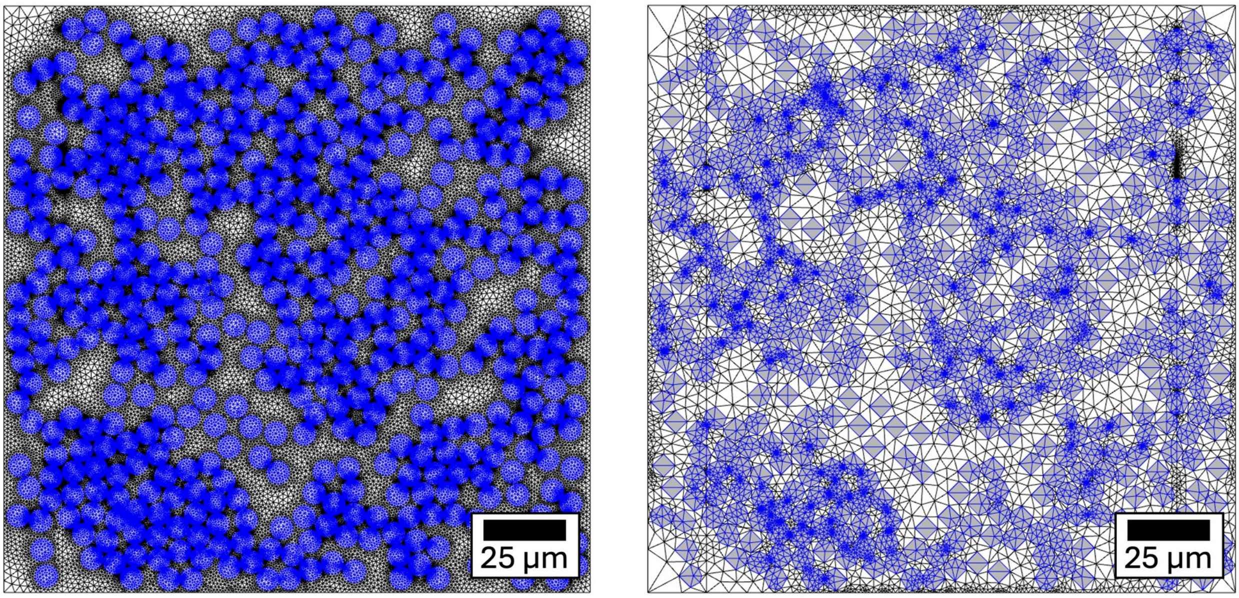

Fig. 1. Representative 2D microscale RVEs with high-fidelity (left) and low-fidelity (right) finite element meshes.

2.4 Multi-fidelity Surrogate Modeling

After collecting sufficient data from the previous step, a multi-fidelity surrogate model was developed using a deep transfer learning (TL) framework. A deep neural network was pre-trained on low-fidelity simulation data to capture the global response of the RVE and subsequently fine-tuned using limited high-fidelity simulation results to capture local mechanistic nuances. In this setup, the pre-trained weights were retained, with retraining -initially applied only to the final output layer. This approach leverages the hierarchical nature of feature extraction that the early layers of a neural network capture general, fundamental features of the design space, while deeper layers specialize in fine-grained, task-specific details [60,61]. By preserving the initial layers, the model retains dominant physical trends from the low-fidelity data, while adapting the final layers to correct the fidelity-dependent bias.

Once the output layer was retrained, additional hidden layers were progressively unfrozen in a layer-wise backward fashion to identify the optimal balance between shared low-fidelity representations and high-fidelity specialization. The architecture consisted of an input layer, ten fully connected hidden layers, and an output layer. Hyperparameters of the initial low-fidelity model were optimized using randomized cross-validation, and model accuracy was assessed using RMSE, MAE, and R^2 metrics. The overall TL process is schematically illustrated in **Fig. 5** below.

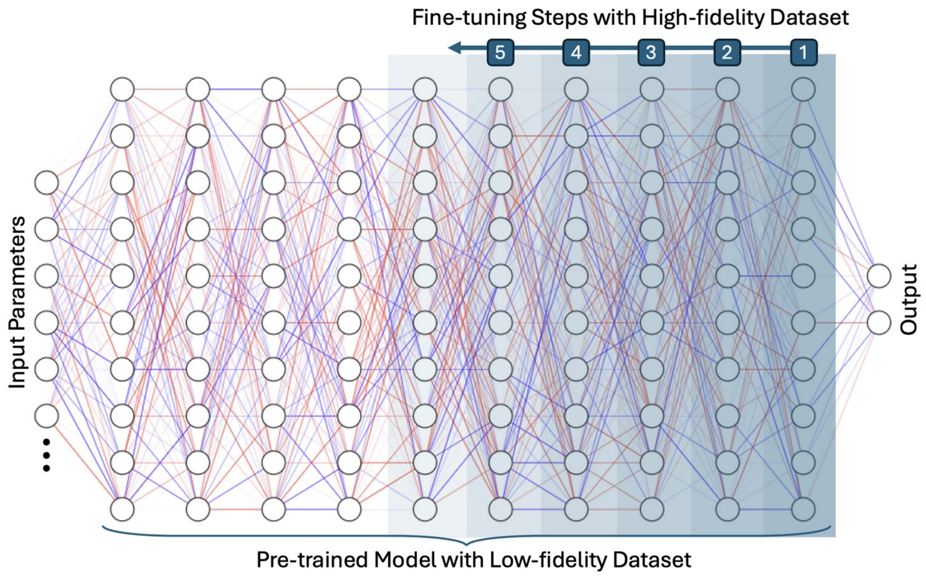

Fig. 1. Schematic illustrating the presented gradual transfer learning process, with retraining initiated at the final (output) layer.

This multi-fidelity surrogate modeling strategy combines the computational efficiency of low-fidelity simulations with the accuracy of high-fidelity data. Pre-training on low-fidelity data enables the model to capture dominant physical trends, while fine-tuning with limited high-fidelity results refines predictive accuracy. This approach improves data efficiency when high-fidelity data are limited and supports surrogate-based uncertainty propagation in subsequent calibration and allowables estimation steps.

2.5 Bayesian MCMC Calibration

Upon training the surrogate model (which can evaluate the forward response in milliseconds), we proceed with Bayesian calibration using MCMC. For this step, we used the Python library *emcee*, which implements the affine-invariant ensemble sampler (i.e., an ensemble of "walkers") proposed by Goodman and Weare (2010) [62]. This sampling strategy in complex multi-parameter spaces. It estimates input parameter distributions by sampling from the Bayesian posterior [63–65]:

$$p(\theta \mid y) \propto p(y \mid \theta)\, p(\theta) \tag{1}$$

In this equation, $p(\theta \mid y)$ is the posterior distribution of input parameters θ given data y, $p(y \mid \theta)$ is the likelihood of observing the data for a given parameter set, and $p(\theta)$ is the prior belief about the parameters before observing the data. In our framework, the surrogate model $M ¿$ serves as the forward operator linking uncertain material and process parameters to the predicted responses used in the calibration. This surrogate-based calibration enables Bayesian inference at a computational cost that would be impractical using direct FE evaluations [66,67].

Priors $p(\theta)$ are chosen as uniform or weakly informative distributions based on physically admissible ranges or prior studies. The ensemble sampler initializes multiple walkers within the prior ranges, performs burn-in, and generates posterior samples. Convergence is assessed using standard chain diagnostics, including integrated autocorrelation time and trace plots. Once posterior samples $\{\theta^{(k)}\}$are obtained, they are propagated through the surrogate to compute posterior predictive distributions of any response quantity [68]:

$$p(q_{new} \mid y) \approx \frac{1}{N_s} \sum_{k=1}^{N_s} M ¿¿ \tag{1}$$

Similar surrogate-accelerated Bayesian methodologies have been successfully demonstrated for progressive damage, viscoplasticity, and multiscale constitutive laws [16,66,69].

VOR: doi.org/10.1016/j.compositesb.2026.114051

2.6 Uncertainty Propagation and Allowables Predictions

With the posterior distributions of the uncertain inputs obtained from MCMC calibration, we propagate these refined uncertainties through the full process simulation chain by re-running the macroscale thermo-chemical cure simulation and microscale thermo-mechanical residual stress estimation. Using the calibrated parameter sets, the curing model recomputes the evolution of degree of cure, modulus, free strains, and the resulting CHILE-based residual stresses, thereby generating process-induced states consistent with the calibrated uncertainties. These updated post-cure properties and residual stresses are then applied in the high-fidelity macroscale failure simulation of the laminate, producing a posterior-consistent strength. This step completes the uncertainty-propagation loop and provides the statistically representative distributions required to estimate A- and B-basis allowables.

For this step of the simulation framework, we used two different models to predict the failure response for macroscale cross-ply laminate. The first model consists of an RVE of two 90-degree plies sandwiched between two 0-degree plies to represent a $[0/90]_{2S}$ laminate. The width of this RVE was chosen as 10 times the thickness of a layer (~1.8-1.9 mm). Each 90-degree ply contains approximately 5000 fibers, while the 0-degree plies were modeled as a homogenized continuum without explicitly modeling fibers. Each simulation at this scale requires approximately 1-2 hours.

A free 2D triangular mesh was generated in COMSOL, consistent with the microscale simulations, for all 0° and 90° plies. A coarser mesh was used in the 0° layers away from the 90° plies. CBFM was employed to simulate failure, with elastic and failure properties of the 0° ply were taken from NCAMP data [12]. For the boundary conditions, nodes on the left side of the RVE were restricted in the horizontal direction, and a tensile displacement was applied to nodes on the right side along the same axis to drive failure in the cross-ply RVE.

The second approach employed in this step utilized the orthotropic continuum damage mechanics model (MAT 261) in LS-DYNA to simulate progressive failure of the $[0/90]_{2S}$ cross-ply coupon. MAT 261 explicitly represents each ply, allowing layer-wise stress redistribution, stiffness degradation, and interlaminar interactions. The formulation incorporates distinct damage variables for fiber and matrix under tension, compression, and shear, with their evolution governed by energy-based criteria linked to constituent strengths and fracture energies.

 VOR: doi.org/10.1016/j.compositesb.2026.114051

This enables differentiation between fiber-dominated and matrix-dominated failures, capturing crack initiation in 90° plies and subsequent load transfer to 0° plies. This model does not explicitly include fiber configurations or local residual stresses; however, inter-ply delamination is captured through tie-break contacts between the adjacent layers. The coupon geometry was divided into three sections of fine and coarse mesh, to reduce the run-time. An illustration of this model is available below in **Fig. 6**. In the fine-mesh region, the element size was set to 0.5╳0.5 mm^2, with one element through the thickness of each layer. In the coarse-mesh regions, the element size was increased to 1.5╳1.5 mm^2, while maintaining one element through the thickness of each layer. Mass scaling and damping were applied to reduce dynamic artifacts and improve convergence, consistent with the explicit LS-DYNA formulation.

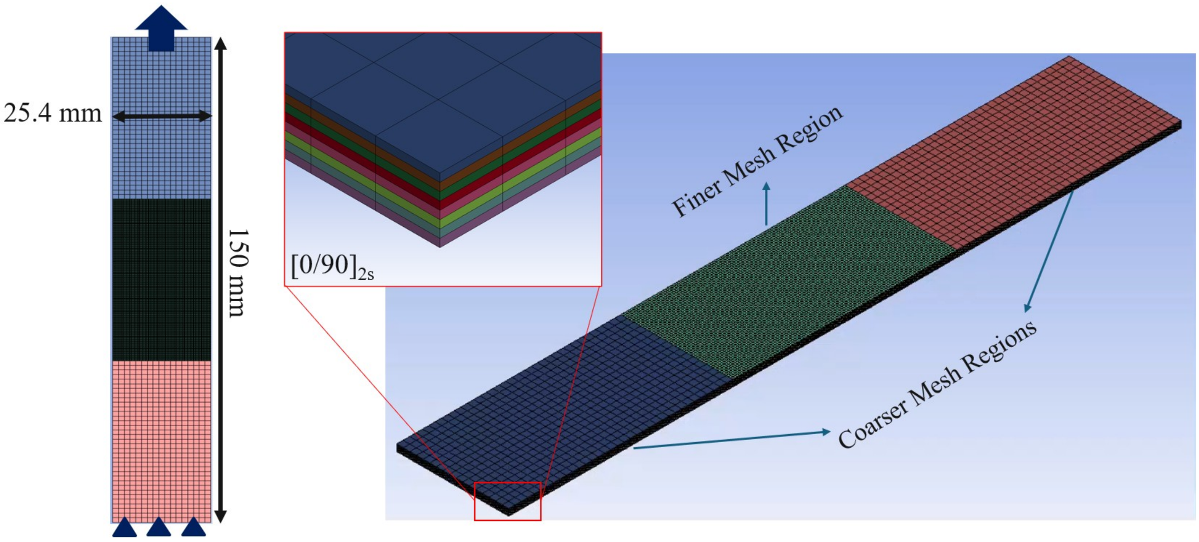

Fig. 1. Illustration of the LS-DYNA cross-ply laminate model. The mesh size is (1.5╳1.5 mm^2) and (0.5╳0.5 mm^2) for the coarser and finer mesh regions respectively. There is one element through the thickness for each layer in both areas.

3 Case Study: AS4/8552 Material System and Models

3.1 Material Description and Modeling Framework

The material system selected for this study is the HEXCEL AS4/8552 unidirectional (UD) prepreg [33,35]. AS4/8552 is a high-performance, aerospace-grade carbon/epoxy system consisting of high-strength AS4 fibers and a toughened 8552 epoxy matrix. The prepreg used in this study has a nominal fiber areal weight of 190 g/m^2 and a nominal resin content of 35% by weight [12]. Its thermo-chemical and thermo-mechanical properties, as well as its translaminar failure characteristics, have been extensively characterized and reported in the

 VOR: doi.org/10.1016/j.compositesb.2026.114051

literature [25–27,34,70–72], making it a representative and well-documented material system for both process and damage simulation.

Statistically robust material properties were sourced from the National Center for Advanced Materials Performance (NCAMP) dataset for Hexcel AS4/8552 [12]. These certification-grade datasets were generated through large multi-batch testing campaigns following, yielding statistical measurements of elastic and failure properties, and corresponding A- and B-basis allowables. Because NCAMP data quantify the inherent material and process variability, they serve as a critical reference for both parameter calibration and validation of probabilistic modeling framework proposed herein.

To simulate the thermo-chemical and thermo-mechanical evolution during the cure cycle, a comprehensive set of state-dependent constitutive models was employed. The process model incorporates equations for cure kinetics and chemical shrinkage, alongside models for thermal conductivity, specific heat capacity and coefficients of thermal expansion. While the fiber properties were defined as temperature-dependent, the matrix properties were modeled as functions of both temperature and the degree of cure. Additionally, a model for glass transition temperature was utilized to govern the transition between the rubbery and glassy states, directly affecting the evolution of resin properties. All governing equations and material parameters were sourced from validated literature for the AS4/8552 material system [34,70,72,73]. This ensures that the framework accurately captures the path-dependent development of material properties and residual stresses.

3.2 Prior Ranges

To implement the Bayesian calibration framework discussed previously, initial prior probability distributions were assigned to the material properties and process parameters. These priors were selected based on a combination of literature data and domain-specific knowledge to ensure the parameters remain within physically admissible bounds. These initial distributions served as the starting point for the stochastic analysis and were subsequently refined through a Bayesian reverse calibration approach using experimental observations and MCMC sampling. The initial stochastic variables and their corresponding prior ranges are summarized in **Table 1**. The output parameters were the RVE modulus and strength, which were trained separately.

Table 1. Prior input distributions

NO.	DEFINITION	NAME	RANGE

1	Heat Transfer Coefficient (Part)	HTC_{part}	$N(60,12)$ [W/(m²K)]
2	Heat Transfer Coefficient (Tool)	HTC_{tool}	$N(40,8)$ [W/(m²K)]
3	Matrix Weight Fraction	W_m	$U(0.343,0.357)$
4	Fiber Aerial Weight	FAW	$U(0.186,0.194)$ [kg/m^2]
5	Matrix Strength	S_m	$U(72,88)$ [MPa]
6	Matrix Fracture Energy	$G_{f,m}$	$U(135,165)$ [J/m^2]
7	Matrix Final Modulus	$E_{m,inf}$	$U(2.925,3.575)$ [GPa]
8	Fiber Longitudinal Modulus	$E_{11,f}$	$U(204.3,249.7)$ [GPa]
9	Fiber Transverse Modulus	$E_{33,f}$	$U(15.48,18.92)$ [GPa]
10	Initial Degree of Cure	x_0	$U(0.005,0.05)$

4 Results and Discussion

4.1 Microscale FE Simulation Results

As described, the process simulation followed a decoupled approach. Initially, the thermo-chemical simulation was conducted to determine the evolution of degree of cure, which subsequently used to calculate the evolution of the resin modulus and process-induced free strains (chemical shrinkage and thermal expansion). Local residual stresses were then calculated within the 2D RVE configuration using the pseudo-viscoelastic CHILE constitutive framework. Residual stresses estimation was performed at both microscale and macroscale levels prior to conducting progressive damage simulations. Representative residual stress distributions are illustrated in **Fig. 7**. Subsequently, failure simulation was performed on the generated RVEs in two fidelities via the CBFM. A total of 1,000 simulations were performed using the low-fidelity model and 200 simulations using the high-fidelity model. Examples of the final failure patterns for both low and high-fidelity simulations are presented in **Fig. 8**.

 VOR: doi.org/10.1016/j.compositesb.2026.114051

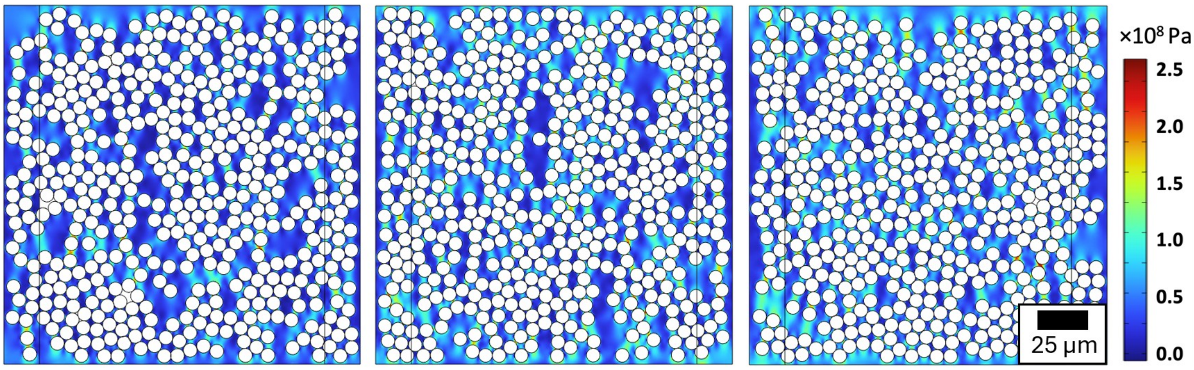

Fig. 1. Examples of predicted process-induced residual stress distributions within the 2D AS4/8552 microscale RVE after the cure cycle.

4.2 Multi-fidelity Surrogate Modeling and Bayesian Calibration Results

i. Global Sensitivity Analysis

Upon establishing the multi-fidelity datasets, a surrogate modeling framework was initiated. To ensure the computational efficiency of the Bayesian inference, a dimensionality reduction was performed. First, a variance-based Global Sensitivity Analysis (GSA) using Sobol' indices was performed to identify the most influential parameters. This analysis was conducted independently for the elastic and failure datasets, and the important parameters were ranked based on their total-effect indices. $E_{33,f}$ and W_m were chosen for elastic surrogate modeling and MCMC calibration, and S_m and $G_{f,m}$ for failure, along with $E_{m,inf}$ which were present in both analyses. **Fig. 9** shows sensitivity analysis results for both RVE modulus and strength.

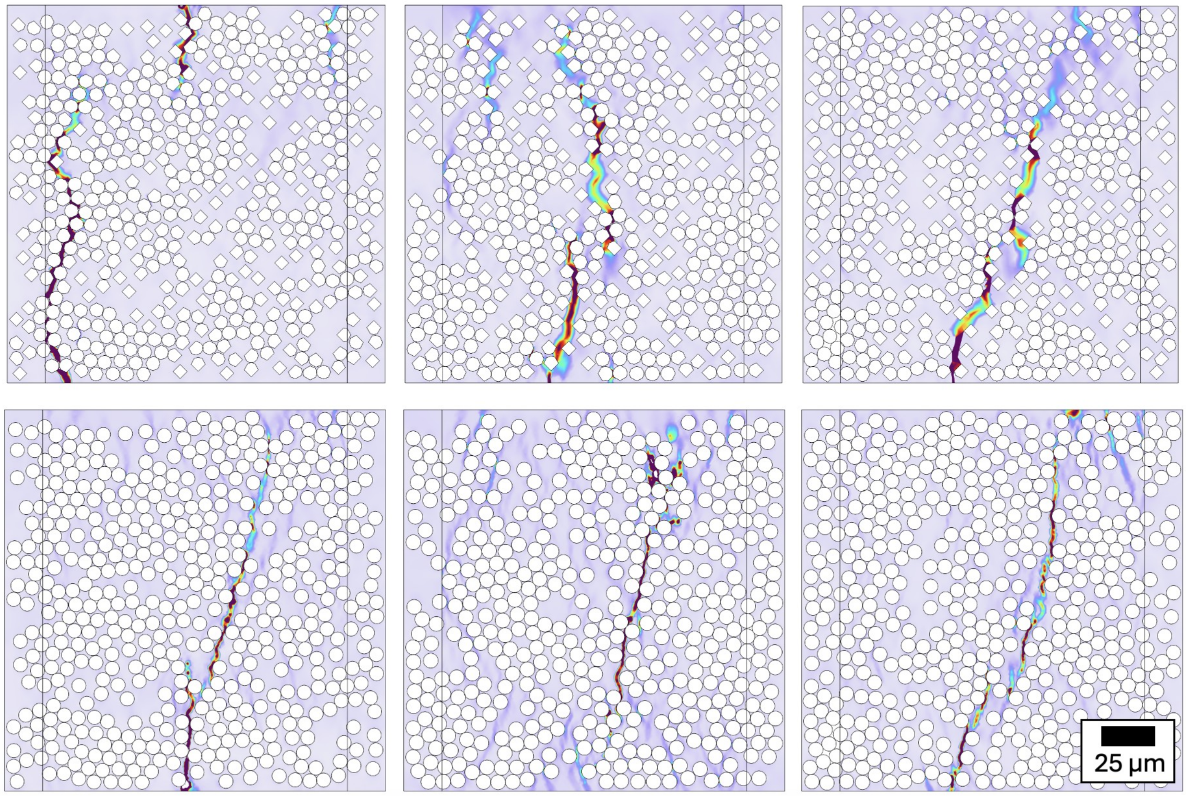

Fig. 1. Comparison of predicted failure morphologies for the AS4/8552 microstructure: low-fidelity (top) and high-fidelity (bottom) CBFM frameworks.

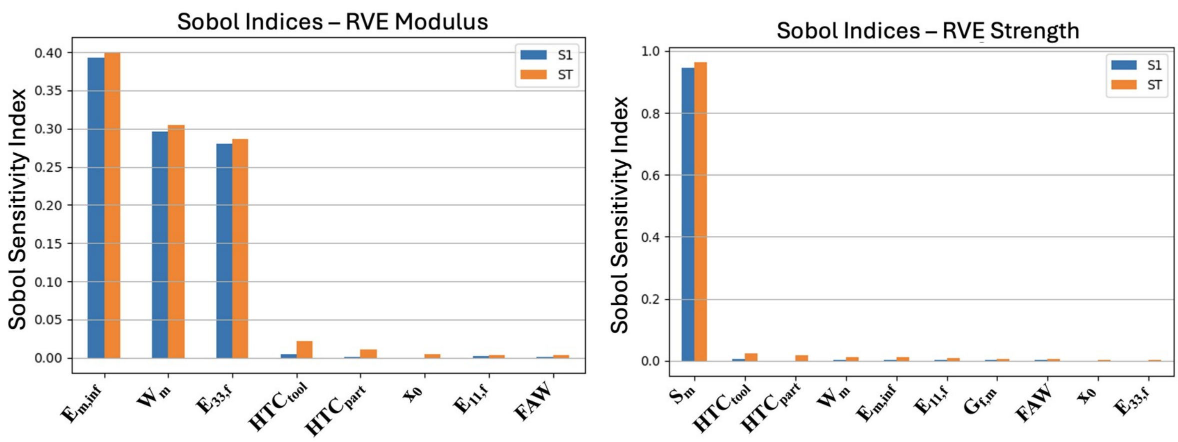

Fig. 1. Sobol' sensitivity indices for the RVE elastic modulus (left) and ultimate strength (right).

ii. Multi-fidelity Surrogate Modeling

Using the reduced parameter set, a multi-fidelity neural network was trained via transfer learning, employing a model trained with the large low-fidelity dataset (n = 1000) as the base architecture. The hyperparameter tuning process was performed on the low-fidelity dataset and then applied to the multi-fidelity neural network. The low fidelity model's hyperparameter ranges and optimized values for predicting RVE strength are listed in **Table 2**.

Table 1. Low-fidelity neural network hyperparameters optimization and training score

Description	Search ranges	Selected values/Score
Activation function for hidden layers	'elu','relu','tanh'	'elu'
Number of neurons per hidden layer	8,16,32,64	16
Learning rate	0.1,0.01,0.001	0.01
Epoch	100,200,300	100
Batch size	16,32,64	64
Optimizer	'Adam'	'Adam'
Loss function	-	'MSE'
Cross-validation size	-	16%
Test size	-	20%
Training Score (R^2)	-	96.2%

To optimize the transfer learning architecture (i.e. the best combination of frozen and retrained layers using high-fidelity data), we divided the 200 high-fidelity dataset into training and validation subsets of equal size. The training subset was used to update the network weights across varying depths of the architecture, while the validation subset was used to assess the accuracy of predictions. The ideal retraining combination was determined by identifying the configuration that yielded the lowest statistical difference between the predicted and validation distributions, as measured by a t-test comparison. The results for the baseline (0 retraining layers) and the optimized combination (4 retraining layers), along with the t-test error values for all architectural combinations, are presented in **Fig. 10**. The lowest t-test error value of approximately 0.2 was observed for 4 retraining layers.

iii. Bayesian Calibration of Parameters

The multi-fidelity surrogate model enabled the efficient execution of iterations using MCMC samplers (ensemble walkers) for inverse parameter inference. In this study, 32 walkers and 1000 steps were employed to reach converged posterior distributions. The results of the Bayesian calibration and corresponding convergence plots are presented in **Fig. 11**.

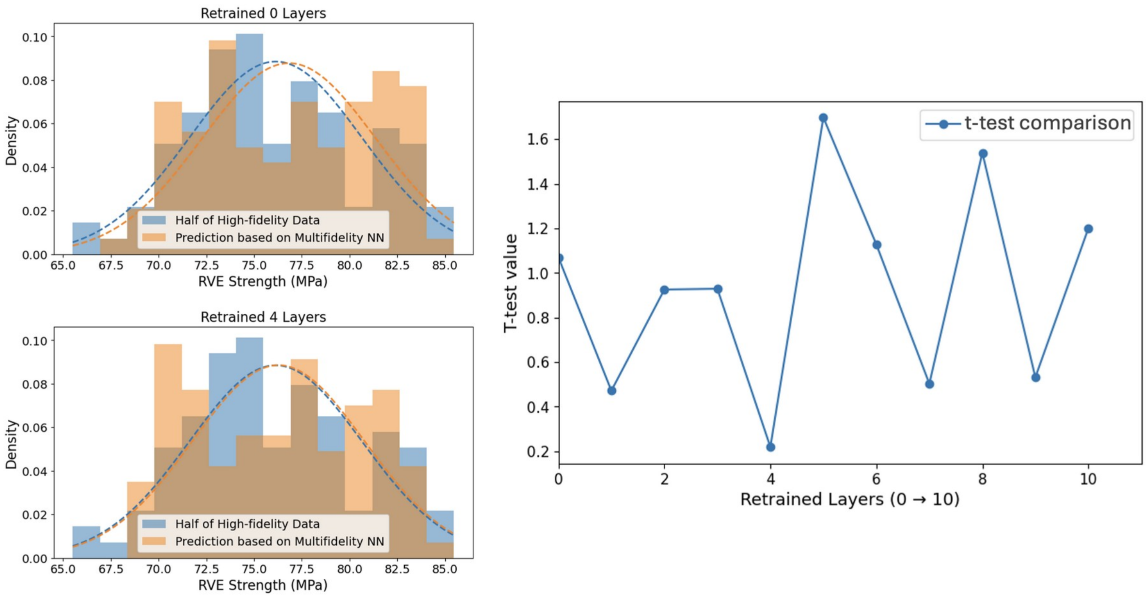

Fig. 1. statistical validation of the multi-fidelity surrogate: (left) comparison of predicted distributions for the baseline (zero retraining) and optimized (4-layer retraining) configurations against the high-fidelity validation set; (right) t-test error values as a function of the number of retrained layers).

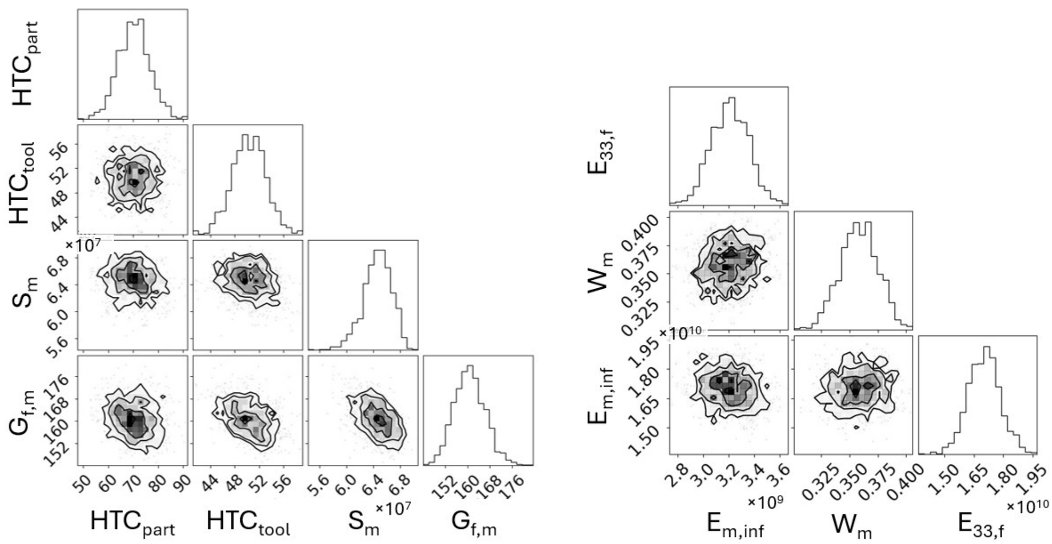

Fig. 1. Inferred posterior distributions of critical input parameters for transverse tension failure (left) and modulus (right).

4.3 Uncertainty Propagation and Allowables Estimation

Fig. 12 shows an example of the macroscale RVE simulation, illustrating two different contours, stress and damage distributions. It is evident that the stress concentration at the tip of transverse cracks acts as the primary site for damage localization and subsequent failure of the 0° plies.

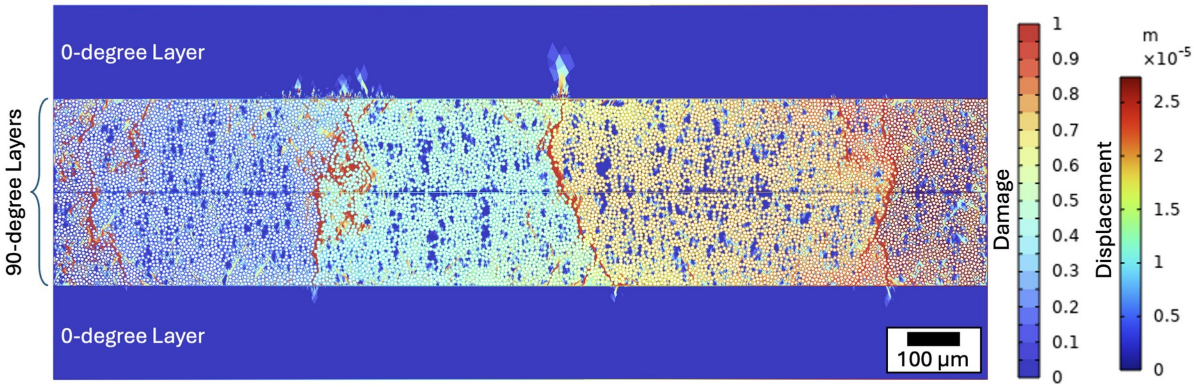

Fig. 1. Predicted failure morphology of the macroscale cross-ply RVE showing damage and displacement contours at the time of ultimate failure.

To generate a stochastic dataset comparable to the NCAMP physical testing (19 experimental tests across 3 batches), uncertainty propagation was performed using 20 realizations each for the RVE and LS-DYNA models, with stochastic input parameters sampled from the derived posterior distributions. The predicted strength distribution is compared against the experimental distribution from NCAMP in **Fig. 13** and **Table 3**, while highlighting the predicted A- and B-basis allowables.

To calculate the A- and B-basis allowables, following equations were used [8]:

$$A_{\text{basis}} = \mu - k_a \times \sigma \tag{1}$$

$$B_{\text{basis}} = \mu - k_b \times \sigma \tag{1}$$

Where μ is the mean value, σ is the standard deviation, and k_a and k_b are the statistical one-sided tolerance factors for the 1st and 10th percentile, respectively, calculated based on the sample size to provide 95% confidence. As shown in **Fig. 13** and **Table 3**, the proposed framework predicts the mean laminate strength with close agreement to the NCAMP data (within 1% of the NCAMP mean). For the standard deviation and resulting allowables, the simulation yields a wider distribution and a more conservative prediction (within 10% of the NCAMP data), which is appropriate for design exploration and risk assessment. However, the predicted allowables are expected to converge toward the experimental values as the sample size increases and the statistical factors (k_a and k_b) are reduced.

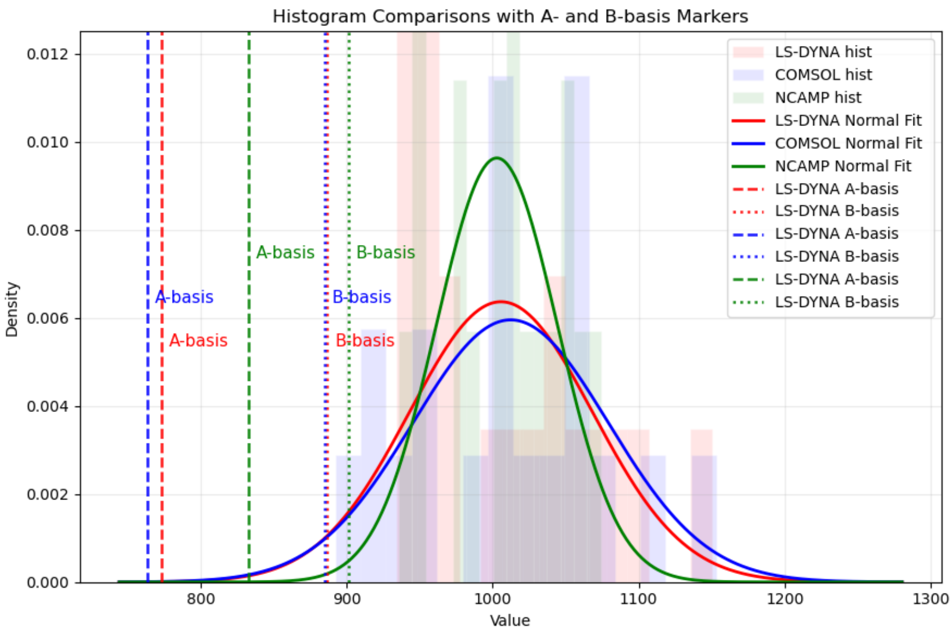

Fig. 1. Comparison of predicted cross-ply strength distributions and NCAMP experimental qualification data.

Table 1. Summary of simulation results and NCAMP experimental benchmark data.

	Experiment (NCAMP)	Present study (COMSOL)	Present study (LS-DYNA)	Error Percentages
Mean	1003 MPa	1012 MPa	1005 MPa	0.9% - 0.2%
Standard Deviation	61 MPa	67 MPa	63 MPa	9.8% - 6.6%
B-basis Allowable	901 MPa	884 MPa	886 MPa	1.9% - 1.7%
A-basis Allowable	833 MPa	763 MPa	772 MPa	8.4% - 7.3%

5 Conclusions

This study introduced a multiscale, multi-fidelity framework for the digital estimation of statistical failure allowables in aerospace composites. By explicitly integrating thermo–chemical/thermo-mechanical process simulations with stochastic multi-fidelity failure analyses, the framework accounts for both constituent-level variability and process-induced effects such as residual stresses. Machine learning surrogate models, optimized via transfer learning, facilitate efficient uncertainty propagation across scales without compromising the underlying physics. A Bayesian inference approach was employed to calibrate stochastic inputs against certification-grade experimental data, thereby incorporating experimentally informed material and process variability.

Validation against the Hexcel AS4/8552 cross-ply laminates from the NCAMP database demonstrated that the framework reproduces mean strength values within 1% of experimental data and provides conservative yet consistent estimates of A- and B-basis allowables within 10% of experimental data. The proposed methodology provides a robust pathway for simulation-informed digital allowables, offering the potential to significantly reduce the cost of experimental qualification campaigns. The physics-informed nature of the approach ensures interpretability, while the multi-fidelity architecture maintains the computational efficiency required for iterative design and risk assessment.

The present study focused on the uncertainty sources explicitly represented in the process–failure framework, including initial degree of cure, prepreg physical-property variability, stochastic RVE morphology, and cure-induced residual stresses. Other manufacturing-induced features, such as porosity, fiber waviness/misalignment, and additional defects affecting 90° and 0° ply failure, were not modeled explicitly in the present implementation. Future work will incorporate these effects and extend the framework to additional loading conditions and lay-ups.

Acknowledgement

We gratefully acknowledge the advising and intellectual support provided by The Boeing Company and the financial support provided by the University of Washington, Materials Science and Engineering Department**,** which enabled the successful execution of this research.

Author contributions: CRediT

Amirali Eskandariyun: Investigation, Methodology, Software, Simulation, Visualization, Validation, Writing – original draft, Writing – review & editing. **Huilong Fu**: Data Curation, Data Analytics, Software, Methodology, Visualization. **Navid Zobeiry**: Conceptualization, Funding acquisition, Methodology, Supervision, Writing – review & editing, Supervision.

References

[1] Ozkan D, Gok MS, Karaoglanli AC. Carbon Fiber Reinforced Polymer (CFRP) Composite Materials, Their Characteristic Properties, Industrial Application Areas and Their Machinability. Advanced Structured Materials 2020;124:235–53. https://doi.org/10.1007/978-3-030-39062-4_20/FIGURES/11.

[2] Zhang J, Lin G, Vaidya U, Wang H. Past, present and future prospective of global carbon fibre composite developments and applications. Compos B Eng 2023;250:110463. https://doi.org/10.1016/J.COMPOSITESB.2022.110463.

[3] Saeedi A, Motavalli M, Shahverdi M. Recent advancements in the applications of fiber-reinforced polymer structures in railway industry—A review. Polym Compos 2024;45:77–97. https://doi.org/10.1002/PC.27817;SUBPAGE:STRING:FULL.

[4] Giurgiutiu V. Structural health monitoring (SHM) of aerospace composites. Polymer Composites in the Aerospace Industry 2015:449–507. https://doi.org/10.1016/B978-0-85709-523-7.00016-5.

[5] Mesogitis TS, Skordos AA, Long AC. Uncertainty in the manufacturing of fibrous thermosetting composites: A review. Compos Part A Appl Sci Manuf 2014;57:67–75. https://doi.org/10.1016/J.COMPOSITESA.2013.11.004.

[6] Billah MM, Elleithy M, Khan W, Yıldız S, Eğer ZE, Liu S, et al. Uncertainty Quantification of Microstructures: A Perspective on Forward and Inverse Problems for Mechanical Properties of Aerospace Materials. Adv Eng Mater 2025;27:2401299. https://doi.org/10.1002/ADEM.202401299;PAGE:STRING:ARTICLE/CHAPTER.

[7] Cox B, Yang Q. In quest of virtual tests for structural composites. Science (1979) 2006;314:1102–7. https://doi.org/10.1126/SCIENCE.1131624/ASSET/A8257CE8-47C0-4526-883F-B2FB03BEBFEF/ASSETS/GRAPHIC/314_1102_F4.JPEG.

[8] International Sae. Composite Materials Handbook 17. SAE International; 2012.

[9] Composite materials handbook. Volume 3, Materials usage, design and analysis 2012:952.

[10] Tomblin J, Ng YC, Raju S. MATERIAL QUALIFICATION AND EQUIVALENCY FOR POLYMER MATRIX COMPOSITE MATERIAL SYSTEMS. 2001.

[11] Schoenholz C, Zappino E, Petrolo M, Zobeiry N. Efficient analysis of composites manufacturing using multi-fidelity simulation and probabilistic machine learning. Compos B Eng 2024;280:111499. https://doi.org/10.1016/J.COMPOSITESB.2024.111499.

[12] Clarkson E. Hexcel 8552 AS4 Unidirectional Prepreg Qualification Statistical Analysis Report FAA Special Project Number SP4614WI-Q Report Release. 2011.

[13] Antin K-N, Laukkanen A, Andersson T, Smyl D, Vilaça P. A Multiscale Modelling Approach for Estimating the Effect of Defects in Unidirectional Carbon Fiber Reinforced Polymer Composites. Materials 2019, Vol 12, Page 1885 2019;12:1885. https://doi.org/10.3390/MA12121885.

[14] Bhattacharyya R, Mahadevan S. Calibration and Validation of Multiscale Model for Ultimate Strength Prediction of Composite Laminates Under Uncertainty. ASCE-ASME Journal of Risk and Uncertainty in Engineering Systems, Part B: Mechanical Engineering 2021;8. https://doi.org/10.1115/1.4053060/1128812.

[15] Vinot M, Liebold C, Usta T, Holzapfel M, Toso N, Voggenreiter H. Stochastic modelling of continuous glass-fibre reinforced plastics–considering material uncertainty in microscale simulations. J Compos Mater 2023;57:133–45. https://doi.org/10.1177/00219983221139790/ASSET/D18DD6BA-7B71-4774-8D7E-091B8E5461FB/ASSETS/IMAGES/LARGE/10.1177_00219983221139790-FIG14.JPG.

[16] Reiner J, Linden N, Vaziri R, Zobeiry N, Kramer B. Bayesian parameter estimation for the inclusion of uncertainty in progressive damage simulation of composites. Compos Struct 2023;321:117257. https://doi.org/10.1016/J.COMPSTRUCT.2023.117257.

[17] Zhou XY, Qian SY, Wang NW, Xiong W, Wu WQ. A review on stochastic multiscale analysis for FRP composite structures. Compos Struct 2022;284:115132. https://doi.org/10.1016/J.COMPSTRUCT.2021.115132.

[18] Li M, Li S, Tian Y, Zhang H, Zhu W, Ke Y. Bottom-up stochastic multiscale model for the mechanical behavior of multidirectional composite laminates with microvoids. Compos Part A Appl Sci Manuf 2024;181:108144. https://doi.org/10.1016/J.COMPOSITESA.2024.108144.

[19] Chen Q, Zhu HH, Ju JW, Guo F, Wang LB, Yan ZG, et al. A stochastic micromechanical model for multiphase composites containing spherical inhomogeneities. Acta Mech 2015;226:1861–80. https://doi.org/10.1007/S00707-014-1278-Y/METRICS.

[20] Khokhar ZR, Ashcroft IA, Silberschmidt V V. Simulations of delamination in CFRP laminates: Effect of microstructural randomness. Comput Mater Sci 2009;46:607–13. https://doi.org/10.1016/J.COMMATSCI.2009.04.004.

[21] Gao Y, Yao H, Wei H, Liu Y. Physics-based deep learning for probabilistic fracture analysis of composite materials. AIAA Scitech 2020 Forum 2020;1 PartF. https://doi.org/10.2514/6.2020-1860.

[22] Bažant ZP, Oh BH. Crack band theory for fracture of concrete. Matériaux et Constructions 1983;16:155–77. https://doi.org/10.1007/BF02486267/METRICS.

[23] Gorgogianni A, Eliaš J, Le JL. Mechanism-Based energy regularization in computational modeling of quasibrittle fracture. Journal of Applied Mechanics, Transactions ASME 2020;87. https://doi.org/10.1115/1.4047207/1083761.

[24] Khalid S, Yazdani MH, Azad MM, Elahi MU, Raouf I, Kim HS. Advancements in Physics-Informed Neural Networks for Laminated Composites: A Comprehensive Review. Mathematics 2025, Vol 13, Page 17 2024;13:17. https://doi.org/10.3390/MATH13010017.

[25] Eskandariyun A, Fu H, Zobeiry N. Integrated Process and Failure Analysis in Composites Using Multi-fidelity Simulations and Machine Learning. American Society for Composites 39th Annual Technical Conference, 2024.

[26] Garstka T, Ersoy N, Potter KD, Wisnom MR. In situ measurements of through-the-thickness strains during processing of AS4/8552 composite. Compos Part A Appl Sci Manuf 2007;38:2517–26. https://doi.org/10.1016/J.COMPOSITESA.2007.07.018.

[27] Zobeiry N, Poursartip A. The origins of residual stress and its evaluation in composite materials. Structural Integrity and Durability of Advanced Composites: Innovative Modelling Methods and Intelligent Design 2015:43 –72. https://doi.org/10.1016/B978-0-08-100137-0.00003-1.

[28] Duffner C, Zobeiry N, Poursartip A. Examination of pre-gelation behaviour in AS4/8552 prepreg composites. 33rd Technical Conference of the American Society for Composites 2018 2018;2:880–92. https://doi.org/10.12783/ASC33/25974.

[29] Elhajjar R. Fat-tailed failure strength distributions and manufacturing defects in advanced composites. Sci Rep 2025;15:1–10. https://doi.org/10.1038/S41598-025-06693-4;SUBJMETA=166,301,639;KWRD=ENGINEERING,MATERIALS+SCIENCE.

[30] Toal DJJ. Applications of multi-fidelity multi-output Kriging to engineering design optimization. Structural and Multidisciplinary Optimization 2023;66:1–21. https://doi.org/10.1007/S00158-023-03567-Z/TABLES/10.

[31] Kennedy MC, O'Hagan A. Predicting the output from a complex computer code when fast approximations are available. Biometrika 2000;87:1–13. https://doi.org/10.1093/BIOMET/87.1.1.

[32] Kulkarni P, Mali KD, Singh S. An overview of the formation of fibre waviness and its effect on the mechanical performance of fibre reinforced polymer composites. Compos Part A Appl Sci Manuf 2020;137:106013. https://doi.org/10.1016/J.COMPOSITESA.2020.106013.

[33] Mehdikhani M, Gorbatikh L, Verpoest I, Lomov S V. Voids in fiber-reinforced polymer composites: A review on their formation, characteristics, and effects on mechanical performance. J Compos Mater 2019;53:1579–669. https://doi.org/10.1177/0021998318772152/ASSET/07D4A013-567C-47C0-AC2E-7BB97D3549E5/ASSETS/IMAGES/LARGE/10.1177_0021998318772152-FIG27.JPG.

[34] Eskandariyun A, Reynolds C, Brunton S, Fu H, Chengalva M, Zobeiry N, et al. A Novel Machine Learning Framework for Digital Estimation of Allowables in Aerospace Composites. Proceedings of ASME 2024 Aerospace Structures, Structural Dynamics, and Materials Conference, SSDM 2024 2024. https://doi.org/10.1115/SSDM2024-121597.

[35] Fu H, Zobeiry N. A Theory-Guided Machine Learning and Reduced-Order Finite Element Modeling Framework to Accelerate Process Simulation of Aerospace Composite Parts. Proceedings of ASME 2023 Aerospace Structures, Structural Dynamics, and Materials Conference, SSDM 2023 2023. https://doi.org/10.1115/SSDM2023-107132.

[36] Higuchi R, Yokozeki T, Nishida K, Kawamura C, Sugiyama T, Miyanaga T. High-fidelity computational micromechanics of composite materials using image-based periodic representative volume element. Compos Struct 2024;328:117726. https://doi.org/10.1016/J.COMPSTRUCT.2023.117726.

[37] Rollet Y, Bonnet M, Carrère N, Leroy FH, Maire JF. Improving the reliability of material databases using multiscale approaches. Compos Sci Technol 2009;69:73–80. https://doi.org/10.1016/J.COMPSCITECH.2007.10.049.

[38] Ghosh G, Biswas D, Bhattacharyya R. Advancements in multiscale modeling of damage in composite materials: A comprehensive review. Compos B Eng 2025;307:112819. https://doi.org/10.1016/J.COMPOSITESB.2025.112819.

[39] Reiner J, Xu X, Zobeiry N, Vaziri R, Hallett SR, Wisnom MR. Virtual characterization of nonlocal continuum damage model parameters using a high fidelity finite element model. Compos Struct 2021;256:113073. https://doi.org/10.1016/J.COMPSTRUCT.2020.113073.

[40] Yan W, Tian X, Liang S, Liang Y, He R, Ai S. Efficient hybrid tensile B-basis value estimation for SiC/SiC composites using sparse testing and high-fidelity digital twin models. J Eur Ceram Soc 2025;45:117351. https://doi.org/10.1016/J.JEURCERAMSOC.2025.117351.

[41] Cardoso RAS, Reis MS, Ferreira LPS, Alves MP, Ha SK, Cimini CA. A-BASIS AND B-BASIS BUCKLING ALLOWABLES FOR AN AIRCRAFT COMPOSITE WING. n.d.

[42] Guo J, Zhang Y, Chen K. Algorithm for Compression Design Allowable Determination of Composite Laminates with Initial Delaminations. Machines 2021, Vol 9, Page 307 2021;9:307. https://doi.org/10.3390/MACHINES9120307.

[43] Zhou K, Enos R, Xu D, Zhang D, Tang J. Hierarchical multi-response Gaussian processes for uncertainty analysis with multi-scale composite manufacturing simulation. Comput Mater Sci 2022;207:111257. https://doi.org/10.1016/J.COMMATSCI.2022.111257.

[44] Gonçalves PT, Arteiro A, Rocha N, Pina L. Numerical Analysis of Micro-Residual Stresses in a Carbon/Epoxy Polymer Matrix Composite during Curing Process. Polymers 2022, Vol 14, Page 2653 2022;14:2653. https://doi.org/10.3390/POLYM14132653.

[45] Kovács N, Rocha IBCM, van der Meer FP, Furtado C, Camanho PP. Uncertainty Quantification in Multiscale Modeling of Polymer Composite Materials Using Physically Recurrent Neural Networks 2025.

[46] Greco F, Leonetti L, Lonetti P, Luciano R, Pranno A. A multiscale analysis of instability-induced failure mechanisms in fiber-reinforced composite structures via alternative modeling approaches. Compos Struct 2020;251:112529. https://doi.org/10.1016/J.COMPSTRUCT.2020.112529.

[47] Husseini JF, Pineda EJ, Stapleton SE. Generation of artificial 2-D fiber reinforced composite microstructures with statistically equivalent features. Compos Part A Appl Sci Manuf 2023;164:107260. https://doi.org/10.1016/J.COMPOSITESA.2022.107260.

[48] Zobeiry N, Vaziri R, Poursartip A. Computationally efficient pseudo-viscoelastic models for evaluation of residual stresses in thermoset polymer composites during cure. Compos Part A Appl Sci Manuf 2010;41:247–56. https://doi.org/10.1016/J.COMPOSITESA.2009.10.009.

[49] Zappino E, Zobeiry N, Petrolo M, Vaziri R, Carrera E, Poursartip A. Analysis of process-induced deformations and residual stresses in curved composite parts considering transverse shear stress and thickness stretching. Compos Struct 2020;241:112057. https://doi.org/10.1016/J.COMPSTRUCT.2020.112057.

[50] Eskandariyun A, Fu H, Stere A, Bauer A, Reynolds C, Chengalva M, et al. A NOVEL MACHINE LEARNING FRAMEWORK FOR DIGITAL ESTIMATION OF ALLOWABLES IN AEROSPACE COMPOSITES 2024.

[51] Comsol. The Structural Mechanics Module User’s Guide. 2019.

[52] Lemaitre J. A Course on Damage Mechanics. A Course on Damage Mechanics 1996. https://doi.org/10.1007/978-3-642-18255-6.

[53] Yosinski J, Clune J, Bengio Y, Lipson H. How transferable are features in deep neural networks? Adv Neural Inf Process Syst 2014;4:3320–8.

[54] Zeiler MD, Fergus R. Visualizing and Understanding Convolutional Networks. Lecture Notes in Computer Science (Including Subseries Lecture Notes in Artificial Intelligence and Lecture Notes in Bioinformatics) 2013;8689 LNCS:818–33. https://doi.org/10.1007/978-3-319-10590-1_53.

[55] Foreman-Mackey D, Hogg DW, Lang D, Goodman J. emcee : The MCMC Hammer . Publications of the Astronomical Society of the Pacific 2013;125:306–12. https://doi.org/10.1086/670067/XML.

[56] Scheiter M. Studies in Monte Carlo Inversion and Generative Deep Learning 2023.

[57] Claudio R:, Cadini SF, Nichetti F, 898993 M. Damage identification in composite panels based on a Bayesian approach and surrogate models 2018.

[58] Seitz G, Mohammadi F, Class H. Thermochemical Heat Storage in a Lab-Scale Indirectly Operated CaO/Ca(OH)2 Reactor—Numerical Modeling and Model Validation through Inverse Parameter Estimation. Applied Sciences 2021, Vol 11, Page 682 2021;11:682. https://doi.org/10.3390/APP11020682.

[59] Adeli E, Rosić B, Matthies HG, Reinstädler S, Dinkler D. Comparison of Bayesian methods on parameter identification for a viscoplastic model with damage. Probabilistic Engineering Mechanics 2020;62:103083. https://doi.org/10.1016/J.PROBENGMECH.2020.103083.

[60] Rappel H, Beex LAA, Hale JS, Noels L, Bordas SPA. A Tutorial on Bayesian Inference to Identify Material Parameters in Solid Mechanics. Archives of Computational Methods in Engineering 2019 27:2 2019;27:361–85. https://doi.org/10.1007/S11831-018-09311-X.

[61] Thijssen B, Wessels LFA. Approximating multivariate posterior distribution functions from Monte Carlo samples for sequential Bayesian inference. PLoS One 2020;15:e0230101. https://doi.org/10.1371/JOURNAL.PONE.0230101.

[62] Hong X, Wang P, Yang W, Zhang J, Chen Y, Li Y. A multiscale Bayesian method to quantify uncertainties in constitutive and microstructural parameters of 3D-printed composites. J Mech Phys Solids 2024;193:105881. https://doi.org/10.1016/J.JMPS.2024.105881.

[63] Shahkarami A, Van Ee D. Material Characterization for Processing: Hexcel 8552 Material Model Development. 2009.